PHYSICAL REVIEW C, VOLUME 61, 011301(R)

Evidence for shears bands in ^{108}Cd

N. S. Kelsall,[1] R. Wadsworth,[1] S. J. Asztalos,[2] B. Busse,[2] C. J. Chiara,[3] R. M. Clark,[2] M. A. Deleplanque,[2] R. M. Diamond,[2] P. Fallon,[2] D. B. Fossan,[3] D. G. Jenkins,[1] S. Juutinen,[4] R. Krücken,[2,*] G. J. Lane,[3,†] I. Y. Lee,[2] A. O. Macchiavelli,[2] C. M. Parry,[1] G. J. Schmid,[2] J. M. Sears,[3] J. F. Smith,[3,‡] F. S. Stephens,[3] K. Vetter,[3] and S. G. Frauendorf[5]

[1]*Department of Physics, York University, Heslington, York Y010 5DD, United Kingdom*

[2]*Nuclear Science Division, Lawrence Berkeley National Laboratory, Berkeley, California 94720*

[3]*Department of Physics and Astronomy, State University of New York, Stony Brook, New York 11794*

[4]*Department of Physics, University of Jyväskylä, SF-40100 Jyväskylä, Finland*

[5]*Department of Physics, University of Notre Dame, Notre Dame, Indiana 46556*

(Received 29 June 1999; published 16 December 1999)

High-spin states were populated in ^{108}Cd using the ^{96}Zr(^{16}O,4n) reaction at a beam energy of 72 MeV. Two magnetic dipole bands have been observed, both of which contain weak $E2$ crossover transitions. Lifetimes for the stronger of the two bands were measured via the Doppler shift attenuation method. The configuration assignment for this band has been determined from comparison with tilted axis cranking model calculations to be $\pi[g_{9/2}^{-3}g_{7/2}]\otimes\nu[h_{11/2}(g_{7/2}d_{5/2})^1]$ and $\pi[g_{9/2}^{-3}g_{7/2}]\otimes\nu[h_{11/2}^3(g_{7/2}d_{5/2})^1]$, before and after the $\nu h_{11/2}^2$ band crossing, respectively. The deduced $B(M1)$ strengths decrease rapidly with increasing spin after the $\nu h_{11/2}^2$ alignment, which is a characteristic behavior of a shears band.

PACS number(s): 21.10.Tg, 23.20.Lv, 25.70.Gh, 27.60+j

Several bands consisting of strong magnetic dipole ($M1$) and weak $E2$ crossover transitions are known to exist in neutron deficient Cd, Sn, and Sb nuclei in the $A\sim110$ mass region. These structures have properties which are very similar to those of magnetic dipole bands in the mass 200 region (e.g., [1]). The bands in the mass 110 region are thought to be based on prolate shapes ($\beta_2\sim0.1$) and have generally been assigned configurations based on one or two holes in the $g_{9/2}$ proton orbital (high-Ω) and particles in the $h_{11/2}$, $g_{7/2}$, and $d_{5/2}$ neutron orbitals (low-Ω) (e.g., see [2–4]). Such considerations make these structures ideal candidates for interpretation within the tilted axis cranking (TAC) model [5]. The important ingredients, as far as this model is concerned, are the proton high-Ω $g_{9/2}$ holes and the high-j, low-Ω $h_{11/2}$ neutrons which, if the collective contribution to the angular momentum is small, results in the total angular momentum lying in a direction tilted with respect to one of the principal axes. Such a coupling naturally breaks the signature symmetry and leads to $\Delta I=1$ sequences (dipole bands). The remaining active protons and neutrons occupy the near degenerate $g_{7/2}$, $d_{5/2}$ shells. Higher angular-momentum states are generated by the proton and neutron spin vectors gradually aligning with the total angular-momentum vector, which lies at some angle with respect to the component vectors. This has been termed the shears mechanism since the action of the vectors resembles the closing of the blades of a pair of shears. A prediction of the TAC model for shears bands is that the $B(M1)$ transition strengths should decrease quite rapidly with increasing spin. This feature has been tested for a wide range of lead nuclei, $^{193-199}$Pb [6,7], through lifetime measurements, but has only been tested in a few cases in the $A\sim110$ mass region [4,8].

Previous work on ^{108}Cd [9] had identified a negative parity $M1$ band with no $E2$ cross-over transitions and a second, weaker structure, consisting of only three transitions, which was not linked to the known decay scheme. These structures were labeled bands 5 and 6, respectively, using the nomenclature of [9]. Band 5 had previously been tentatively assigned a $\pi g_{9/2}^{-2}\otimes\nu[h_{11/2}(g_{7/2},d_{5/2})^3]$ configuration at low spin, however, the present work is in disagreement with this interpretation. Both of these structures have been observed and extended in the present work. Lifetimes have been extracted for band 5 by means of the Doppler shift attenuation method (DSAM) and the deduced $B(M1)$ values have been compared with the predictions of the TAC model. Above the $\nu h_{11/2}^2$ alignment in this band, the results are consistent with those expected from a shears type mechanism, thus providing further support for this excitation mode in this mass region.

High-spin states in ^{108}Cd were populated via the ^{96}Zr(^{16}O,4n) fusion-evaporation reaction channel at a beam energy of 72 MeV. The target consisted of a 500 μg/cm^2 enriched (86%) ^{96}Zr foil mounted upon a 10 mg/cm^2 thick natural lead backing. Gamma rays were detected using the GAMMASPHERE multidetector array which contained 99 large volume HPGe detectors for this experiment. Approximately 5×10^8 events were recorded with a suppressed Ge fold $\geqslant4$. These data were then unpacked into triples and sorted into an E_γ-E_γ-E_γ cube, and analyzed using the Radware analysis package LEVIT8R [10]. These data were also sorted into γ-gated matrices with all angles on one axis and specific angles on the other axis for use in the lifetime analysis. In this latter case the gates were set on fully stopped transitions at the bottom of, and directly below the band of interest. Two further γ-gated matrices were sorted, one con-

*Present address: Wright Nuclear Structure Laboratory, Physics Department, Yale University, New Haven, CT 06520.

†Present address: Nuclear Science Division, Lawrence Berkeley National Laboratory, Berkeley, CA 94720.

‡Present address: Nuclear Physics Group, Schuster Laboratory, University of Manchester, Brunswick Street, Manchester M13 9PL, U.K.

TABLE I. Spectroscopic details for transitions in bands 5 and 6. Mean lifetimes and reduced transition strengths are given for those levels for which the DSAM was applied. Pure $M1$ character was assumed for the $\Delta I=1$ transitions when calculating the $B(M1)$ values.

E_γ (keV)	Intensity	DCO	Multipolarity	$I_i^\pi \rightarrow I_f^\pi$	τ (ps)	$B(M1)$ $[\mu_N^2]$	$B(E2)$ $[e^2b^2]$
121.0	60.6 ± 2.4	$0.85^{+0.07}_{-0.07}$	$M1$	$13^-\rightarrow12^-$	-	-	-
212.0	8.4 ± 0.5	$0.64^{+0.1}_{-0.1}$	$M1/E2$	$17^-\rightarrow16^-$	-	-	-
284.4	7.9 ± 0.7	$0.71^{+0.08}_{-0.08}$	$M1$	$19^-\rightarrow18^-$	-	-	-
314.0	8.4 ± 0.9	$0.86^{+0.1}_{-0.1}$	$M1$	$16^-\rightarrow(15^-)$	-	-	-
316.0	85.5 ± 3.1	$0.75^{+0.03}_{-0.04}$	$M1$	$14^-\rightarrow13^-$	-	-	-
323.4	19.9 ± 1.0	$0.86^{+0.07}_{-0.07}$	$M1$	$19^-\rightarrow18^-$	-	-	-
333.0	5.4 ± 0.5	$0.68^{+0.4}_{-0.3}$	$M1$	$17^-\rightarrow16^-$	-	-	-
358.8	26.4 ± 2.0	$0.65^{+0.06}_{-0.04}$	$M1$	$(20^-)\rightarrow19^-$	-	-	-
361.7	41.5 ± 1.7	$0.82^{+0.05}_{-0.04}$	$M1$	$18^-\rightarrow17^-$	$0.75^{+0.05}_{-0.06}$	$1.6^{+0.1}_{-0.1}$	-
420.8	13.9 ± 1.8	$0.73^{+0.09}_{-0.08}$	$M1$	$(21^-)\rightarrow(20^-)$	-	-	-
455.4	11.6 ± 0.7	-	$(M1)$	$18^-\rightarrow17^-$	-	-	-
465.5	22.3 ± 1.2	$0.97^{+0.12}_{-0.1}$	$M1$	$17^-\rightarrow16^-$	$0.40^{+0.05}_{-0.05}$	$0.8^{+0.1}_{-0.1}$	-
476.6	9.1 ± 0.4	$0.9^{+0.14}_{-0.13}$	$M1$	$(22^-)\rightarrow(21^-)$	-	-	-
482.3	30.6 ± 1.5	$1.00^{+0.03}_{-0.04}$	$M1$	$19^-\rightarrow18^-$	$0.29^{+0.02}_{-0.02}$	$1.5^{+0.1}_{-0.1}$	-
492.0	4.8 ± 0.5	$0.6^{+0.1}_{-0.1}$	$M1/E2$	$18^-\rightarrow17^-$	-	-	-
515.6	-	-	$(M1)$	$(23^-)\rightarrow(22^-)$	-	-	-
520.0	4.8 ± 0.2	$0.87^{+0.07}_{-0.06}$	$M1/E2$	$18^-\rightarrow17^-$	-	-	-
521.7	100	$0.8^{+0.03}_{-0.02}$	$M1$	$15^-\rightarrow14^-$	$0.69^{+0.04}_{-0.06}$	$0.58^{+0.06}_{-0.04}$	-
527.0	9.6 ± 0.8	$1.21^{+0.15}_{-0.18}$	$M1/E2$	$17^-\rightarrow(15^-)$	-	-	-
558.0	1.6 ± 0.3	-	$(M1/E2)$	$18^-\rightarrow17^-$	-	-	-
563.6	6.5 ± 1.4	$0.79^{+0.08}_{-0.08}$	$M1$	$(24^-)\rightarrow(23^-)$	-	-	-
589.5	9.0 ± 1.0	$0.73^{+0.01}_{-0.09}$	$M1$	$20^-\rightarrow19^-$	$0.20^{+0.03}_{-0.04}$	$1.1^{+0.2}_{-0.2}$	-
615.0	13.5 ± 0.7	$0.69^{+0.15}_{-0.13}$	$M1/E2$	$(15^-)\rightarrow15^-$	-	-	-
676.7	22.1 ± 0.9	$0.78^{+0.1}_{-0.1}$	$M1$	$16^-\rightarrow15^-$	$0.27^{+0.06}_{-0.09}$	$0.7^{+0.3}_{-0.1}$	-
682.0	4.4 ± 0.4	$1.47^{+0.12}_{-0.11}$	$E2$	$(20^-)\rightarrow18^-$	-	-	-
705.6	7.0 ± 0.4	$0.75^{+0.05}_{-0.04}$	$M1$	$21^-\rightarrow20^-$	$0.30^{+0.01}_{-0.01}$	$0.40^{+0.06}_{-0.04}$	-
780.4	3.2 ± 0.3	-	$(E2)$	$(21^-)\rightarrow19^-$	-	-	-
797.9	5.1 ± 0.4	-	$(M1)$	$(22^-)\rightarrow21^-$	-	-	-
45.0	3.3 ± 0.3	$1.31^{+0.17}_{-0.15}$	$E2$	$19^-\rightarrow17^-$	-	-	$0.07^{+0.05}_{-0.05}$
897.8	2.7 ± 0.4	-	$(E2)$	$(22^-)\rightarrow(20^-)$	-	-	-
931.0	7.8 ± 0.5	$0.94^{+0.2}_{-0.2}$	$M1/E2$	$16^-\rightarrow15^-$	-	-	-
993.6	4.0 ± 0.5	$1.5^{+0.4}_{-0.3}$	$E2$	$(23^-)\rightarrow(21^-)$	-	-	-
1073.9	2.6 ± 0.3	-	$(E2)$	$20^-\rightarrow18^-$	-	-	$0.06^{+0.04}_{-0.04}$
1079.0	2.8 ± 0.3	-	$(E2)$	$(24^-)\rightarrow(22^-)$	-	-	-
1293.6	2.5 ± 0.3	-	$(E2)$	$21^-\rightarrow19^-$	-	-	$0.02^{+0.01}_{-0.01}$
1337.1	7.1 ± 0.5	$0.93^{+0.2}_{-0.2}$	$E1$	$17^-\rightarrow16^+$	-	-	-
1404.1	3.3 ± 0.3	$0.7^{+0.16}_{-0.14}$	$E1$	$17^-\rightarrow16^+$	-	-	-
1502.2	1.6 ± 0.3	-	$(E2)$	$(22^-)\rightarrow20^-$	-	-	-

taining a combination of detectors at the angles 29° and 151° relative to the beam direction on both the x and y axes, and the other containing these angles on the y axis, but with the detectors at 90° on the x axis. This enabled directional correlation ratios [11] to be deduced for the γ rays of interest. These ratios were compared to the measured values of known stretched $E2\leftrightarrow$ stretched $E2$ and stretched $E2\leftrightarrow$ stretched dipole transitions, which were found to be 1.48 and 0.77, respectively, after correction for the number of detectors at each angle. Directional correlation with oriented nuclei technique (DCO) ratios for both dipole bands are presented in Table I.

The partial level scheme deduced from the present work is shown in Fig. 1. Intensity balance arguments support the magnetic dipole character of the $\Delta I=1$ transitions in bands 5 and 6. We have extended band 5 by one extra $M1$ transition. In addition, we have observed several weak $E2$ crossover transitions within the band. Band 6 has been extended considerably, with the inclusion of nine new $M1$ transitions and the observation of very weak $E2$ crossover transitions. This dipole band has also been linked to the level scheme via feeding into the yrast band and band 5.

Only band 5 could be gated upon cleanly enough to enable lifetimes to be measured. Lifetimes were extracted for

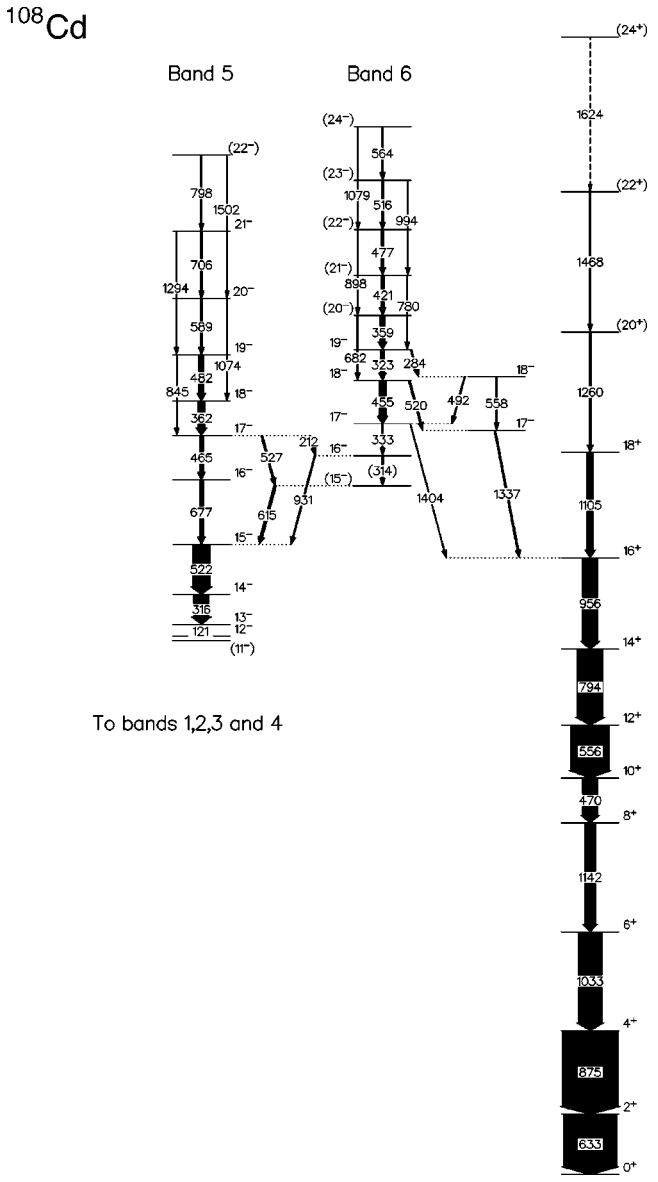

FIG. 1. Partial level scheme showing the two dipole bands (5 and 6) which have been extended as a result of this work. The drop in intensity of the gamma transition at spin 10^+ in the yrast band results from the decay out of this state to other known structures (see Thorslund *et al.* [9]).

states in the band using the program ''LINESHAPE'' written by Wells and Johnson [12]. The detailed slowing down process of the recoils within the target and backing was simulated using a Monte Carlo technique, using 5000 histories with a time step of 0.001 ps. The slowing down process was treated according to the prescription given by Gascon *et al.* [13]. The tabulations of Northcliffe and Schilling [14], with shell corrections, were used for the electronic stopping powers. These histories were then used to produce the velocity distribution observed by each angular group of detectors. Line shapes were fitted simultaneously to forward, backward, and transverse spectra. The detectors used in the analysis were located at angles of 31.7° (5), 37.4° (5), 50.1° (10), 58.3° (5), 90.0° (8), 121.7° (5), 129.9° (10), 142.6° (5), and

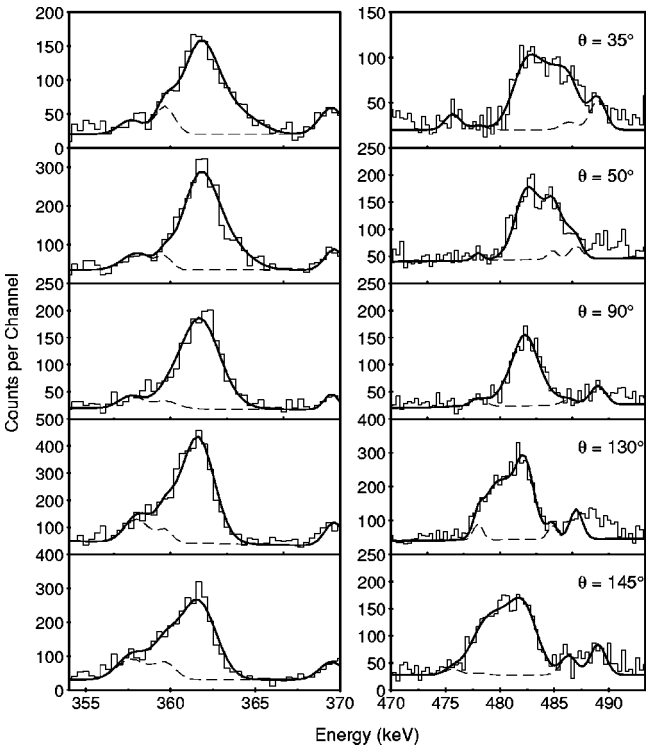

FIG. 2. Experimental data and line shape fits for the 362 keV and 482 keV transitions in band 5, left and right, respectively. The dashed lines show the positions and intensities of contaminant peaks.

148.3° (5); the parentheses refer to the number of detectors located at each angle. Separate fits were performed for detectors located at averaged angles of 52.8°, 90°, 127.2° and 34.6°, 90.0°, 145.4°. The fits were all performed assuming that feeding into each state, including the topmost level, was via a rotational cascade of five transitions with a moment of inertia of $10\hbar^2(\mathrm{MeV})^{-1}$. The side-feeding moment of inertia was varied and found to have a negligible effect on the extracted lifetimes once the actual fits were of reasonable quality. An intensity profile for the side feeding was estimated from the backed target data. The effective lifetime of the topmost state was determined and then fixed and used as an input parameter for a global fit of the entire cascade. Final results came from this global fit with independently variable lifetimes for each state and the associated side feeding. The side-feeding lifetimes were found to be up to two to four times faster than the in-band lifetimes. Typical line-shape fits are shown in Fig. 2. The mean lifetimes for states in band 5 are presented in Table I along with the $B(M1)$ transition strengths.

Thorslund *et al.* [9] tentatively assigned the structure of band 5 as $\pi g_{9/2}^{-2} \otimes \nu[h_{11/2}(g_{7/2}d_{5/2})^3]$ and $\pi g_{9/2}^{-2} \otimes \nu[h_{11/2}^3(g_{7/2}d_{5/2})^3]$ before and after the $\nu h_{11/2}^2$ band crossing, respectively. At first sight this is not unreasonable since a configuration involving two $g_{9/2}$ holes has been assigned to the dipole band in ^{110}Cd [4]. However, the $B(M1)$ transition strengths in the ^{110}Cd band are considerably larger (~ 2–$5\mu_N^2$) than those observed in the present work. The TAC calculations for the previously assigned configuration

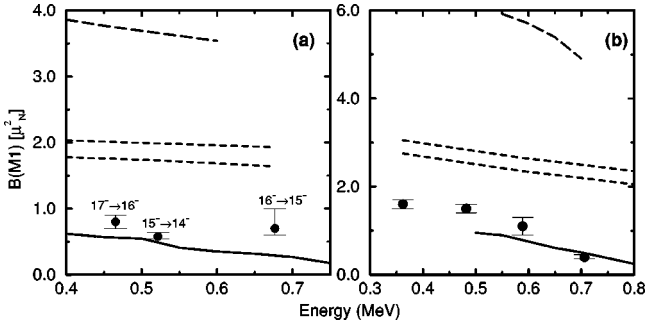

FIG. 3. Comparison of TAC and Dönau and Frauendorf model predictions for $B(M1)$ values with the experimentally deduced values (filled circles) for band 5. (a) TAC predictions (solid line) for the $\pi[g_{9/2}^{-3}g_{7/2}]\otimes\nu[h_{11/2}(g_{7/2}d_{5/2})^1]$ configuration together with the experimental data below the $\nu h_{11/2}^2$ band crossing. (b) TAC predictions (solid line) for the $\pi[g_{9/2}^{-3}g_{7/2}]\otimes\nu[h_{11/2}^3(g_{7/2}d_{5/2})^1]$ configuration together with the experimental $B(M1)$ values above the $\nu h_{11/2}^2$ band crossing. Note that the calculations do not extend to low frequency because of the difficulty in identifying the configuration below 0.5 MeV. The long-dashed line shows the TAC predictions for the $\pi g_{9/2}^{-2}\otimes\nu[h_{11/2}(g_{7/2}d_{5/2})^1]$ and $\pi g_{9/2}^{-2}\otimes\nu[h_{11/2}^3(g_{7/2}d_{5/2})^1]$ configurations in (a) and (b), respectively. The dashed lines show Dönau and Frauendorf predictions for the $\pi[g_{9/2}^{-3}g_{7/2}]\otimes\nu[h_{11/2}(g_{7/2}d_{5/2})^1]$ and $\pi[g_{9/2}^{-3}g_{7/2}]\otimes\nu[h_{11/2}^3(g_{7/2}d_{5/2})^1]$ configurations in (a) and (b), respectively. The two lines show the extreme limits of the $B(M1)$ values depending on whether the $g_{7/2}$ or $d_{5/2}$ neutron g factor is used.

also produce $B(M1)$ values which are approximately three times greater than the experimental values (see Fig. 3). These results suggest that band 5 is not based on a $\pi g_{9/2}^{-2}$ configuration. ^{106}Cd contains a negative parity dipole band which has been assigned a configuration based upon three $g_{9/2}$ proton holes and one $g_{7/2}$ proton, i.e., a $g_{9/2}$ proton is excited into the $g_{7/2}$ proton orbital [15]. Such a configuration would be expected to have lower $B(M1)$ values because two of the proton holes may align antiparallel and therefore not contribute to the shears mechanism or the magnetic dipole moment. It is possible that a similar configuration may be responsible for band 5 in ^{108}Cd.

The $\pi[g_{9/2}^{-3}g_{7/2}]\otimes\nu[h_{11/2}(g_{7/2}d_{5/2})^1]$ configuration would be expected to have a band-head spin of $\sim$12–13$\hbar$, assuming the perpendicular coupling of the $g_{9/2}$ proton hole ($3.5\hbar$) along one axis and the remaining $h_{11/2}$, $(g_{7/2},d_{5/2})$ neutron particles, and the $g_{7/2}$ proton along the other axis. This is in good agreement with the observed bandhead spin for band 5. Following the $\nu h_{11/2}^2$ alignment the configuration for this structure becomes $\pi[g_{9/2}^{-3}g_{7/2}]\otimes\nu[h_{11/2}^3(g_{7/2}d_{5/2})^1]$.

TAC [5] calculations were performed for the above configurations. These predict $B(M1)$ transition strengths in much closer agreement with the experimental values than calculations for the $\pi g_{9/2}^{-2}$ configuration (see Fig. 3). The bandhead for the $\pi[g_{9/2}^{-3}g_{7/2}]\otimes\nu[h_{11/2}^3(g_{7/2}d_{5/2})^1]$ configuration is predicted to lie at an excitation energy of 1.92 MeV relative to that for the $\pi[g_{9/2}^{-3}g_{7/2}]\otimes\nu[h_{11/2}(g_{7/2}d_{5/2})^1]$ configuration. This agrees reasonably well with the experimental excitation energy of 2.1 MeV. The deformations used in the calculations ($\beta_2=0.14$, $\gamma=-125°$) were obtained by minimizing with respect to energy in the $\beta_2-\gamma$ plane using a value for κ, the Q-Q coupling constant, scaled by $A^{5/3}$ from that used for the TAC calculations in the lead region [7]. Note however that the $B(E2)$ value appears to decrease markedly from the 20^- to the 21^- state (see Table 1). This implies a reduction in deformation towards the top of the band. If the deformation were to decrease, then the $B(M1)$ values would fall off faster with increasing spin. However, this effect cannot be taken into account in the current TAC model as the deformation is fixed for a given configuration.

TABLE II. Calculated shears angle θ and proton angle θ_π for states in band 5.

E_γ (keV)	I_i^π	θ (°)	θ_π (°)
121.0	13^-	81.2	65.1
316.0	14^-	71.0	57.1
521.7	15^-	61.6	48.4
676.7	16^-	49.7	38.7
361.7	18^-	79.8	68.4
482.3	19^-	68.7	58.4
589.5	20^-	56.4	47.5
705.6	21^-	41.4	34.5
797.9	22^-	17.6	14.4

$B(E2)$ values were determined using the expression given in Ref. [16]. If the nucleus is assumed to be axially symmetric then standard expressions can be used to determine β_2 [17]. From such an analysis, β_2 was calculated to be $0.11^{+0.06}_{-0.07}$ for the two lowest $E2$ transitions, and $0.06^{+0.02}_{-0.02}$ for the highest $E2$ transition (see Table I). The initial values are in reasonable agreement with the β_2 deformation parameter deduced from the TAC model calculations (0.14), thus confirming the weakly deformed nature of the nucleus for these structures.

The semiclassical Dönau and Frauendorf formalism [18] was also applied to band 5 using the two configurations discussed above. This geometric model predicts $B(M1)$ values which are somewhat larger than the experimental results and the TAC model predictions. Moreover, the geometric model predictions do not fall off as rapidly as the experimental values at high frequency (see Fig. 3). We therefore conclude that the TAC model better predicts the behavior of this dipole band in ^{108}Cd and that the structure of the band is most likely based on $\pi[g_{9/2}^{-3}g_{7/2}]\otimes\nu[h_{11/2}(g_{7/2}d_{5/2})^1]$ and $\pi[g_{9/2}^{-3}g_{7/2}]\otimes\nu[h_{11/2}^3(g_{7/2}d_{5/2})^1]$ configurations before and after the $\nu h_{11/2}$ band crossing, respectively. The present results strongly suggest that the shears mechanism is active following the $\nu h_{11/2}^2$ alignment in this band. Experimentally, the evidence is not so clear for the mechanism below the band crossing. The presence of the shears mechanism is perhaps surprising given that the component vectors for the aligned configuration are of rather unequal length.

A more phenomenological description of the shears mechanism has recently been presented in terms of the coupling of two long vectors $\mathbf{j}_\pi$ and $\mathbf{j}_\nu$ [19,20], their interaction being mediated by an effective quadrupole force attributed to

particle-vibration coupling. Assuming that these rigid shears close as the spin increases, it is possible to calculate the shears angle, θ, between the two vectors $\mathbf{j}_\pi$ and $\mathbf{j}_\nu$, and the proton angle, θ_π, the angle between the total angular momentum vector $\mathbf{J}$, and the proton vector $\mathbf{j}_\pi$. Previous calculations using this model, performed for ^{106,108}Sn, assumed that the contribution of the core rotation to $\mathbf{J}$ was negligible. TAC calculations for ^{108}Cd show that there are more proton particle-hole excitations, which also have much larger amplitudes, for structures which have analogous configurations and deformations to those in ^{108}Sn. This gives rise to a larger collective core contribution in the Cd nuclei. The effect of the core contribution due to the deformation is to retard the closure of the shears and also to allow more angular momentum to be generated in total. The total spin generated from the two mechanisms may be decomposed into I_{shears} and R_{core}, the angular momentum contributions from the shears and core, respectively. It is assumed that R_{core} increases linearly from zero at the bandhead to a maximum value at the top of the band. This is then assumed to be equal to the difference between the total spin of the band and that which may be generated from the shears alone. At the top of band 5 in ^{108}Cd the fraction of the total spin generated by the core contribution is small ($\sim$10%). This results from the fact that the maximum spin obtainable from the configuration, when the shears are closed, is 20 and the band is observed up to spin 22. Once this linear contribution is subtracted, the shears and proton angles may be calculated from simple geometry in the manner outlined in Ref. [8]. The results are presented in Table. II. The angles decrease for the configurations above and below the band crossing with increasing spin, however, experimentally, we only have lifetime data for two states below the $\nu h_{11/2}$ band crossing. This makes it difficult to be certain as to whether the shears mechanism is really active in this region.

Band 6 has also been tentatively assigned negative parity from the DCO ratios obtained for the linking transitions with band 5 and the yrast band. With this assumption the configuration for this band is probably very similar to that of band 5 but with an additional pair of $g_{7/2}d_{5/2}$ neutrons, i.e., a $\pi[g_{9/2}^{-3}g_{7/2}]\otimes\nu[h_{11/2}(g_{7/2}d_{5/2})^3]$ configuration at the bandhead. Such a configuration would be expected to have an initial spin of $\sim$17–18$\hbar$, assuming perpendicular coupling, which is in good agreement with the observed spin.

In summary, two dipole bands have been observed in ^{108}Cd. Lifetimes have been extracted for levels in the more strongly populated structure (band 5). The deduced $B(M1)$ transition strengths have confirmed that the band has the characteristics of a shears band above the $\nu h_{11/2}^2$ alignment and, furthermore, TAC calculations suggest that the configuration is $\pi[g_{9/2}^{-3}g_{7/2}]\otimes\nu[h_{11/2}(g_{7/2}d_{5/2})^1]$ and $\pi[g_{9/2}^{-3}g_{7/2}]\otimes\nu[h_{11/2}^3(g_{7/2}d_{5/2})^1]$, before and after the band crossing, respectively. A configuration of $\pi[g_{9/2}^{-3}g_{7/2}]\otimes\nu[h_{11/2}(g_{7/2}d_{5/2})^3]$ is tentatively suggested for band 6.

The authors would like to thank the staff at the 88-Inch Cyclotron for providing the beam. We would also like to thank John Wells for providing the lineshape analysis package. This work has been supported by the U.K. EPSRC, U.S. NSF, and Department of Energy under Contract No. DE-AC03-76SF00098.

[1] S. Frauendorf, Rev. Mod. Phys. (to be submitted).
[2] D.G. Jenkins *et al.*, Phys. Lett. B **428**, 23 (1998).
[3] D.G. Jenkins *et al.*, Phys. Rev. C **58**, 2703 (1998).
[4] R.M. Clark *et al.*, Phys. Rev. Lett. **82**, 3220 (1999).
[5] S. Frauendorf, Nucl. Phys. **A557**, 259c (1993).
[6] R.M. Clark *et al.*, Phys. Rev. Lett. **78**, 1868 (1997).
[7] R.M. Clark *et al.*, Phys. Lett. B **440**, 251 (1998).
[8] D.G. Jenkins *et al.*, Phys. Rev. Lett. **83**, 500 (1999).
[9] I. Thorslund *et al.*, Nucl. Phys. **A564**, 285 (1993).
[10] D.C. Radford, Nucl. Instrum. Methods Phys. Res. A **361**, 297 (1995).
[11] K.S. Krane, R.M. Steffen, and R.M. Wheeler, Nucl. Data Tables **11**, 351 (1973).
[12] J.C. Wells and N.R. Johnson, Lineshape: A Computer Program for Doppler-broadened Lineshape Lifetime Analysis (1994).
[13] J. Gascon *et al.*, Nucl. Phys. **A513**, 344 (1990).
[14] L.C. Northcliffe and R.F. Schilling, Nuclear Data Tables **A7**, 233 (1970).
[15] P.H. Regan *et al.*, Nucl. Phys. **A586**, 351 (1995).
[16] H. Ejiri and M.J.A. de Voigt, *Gamma-Ray and Electron Spectroscopy in Nuclear Physics* (Oxford University Press, Oxford, England, 1989), p. 504.
[17] R.B. Firestone, *Table of Isotopes*, 8th ed. (John Wiley & Sons, New York, 1996), Vol. 2.
[18] F. Dönau and S. Frauendorf, in Proceedings of the International Conference on High Angular Momentum Properties of Nuclei, Oak Ridge, 1983, edited by N.R. Johnson, p. 143.
[19] A.O. Macchiavelli, R.M. Clark, M.A. Deleplanque, R.M. Diamond, P. Fallon, I.Y. Lee, F.S. Stephens, K. Vetter, Phys. Rev. C **57**, R1073 (1998).
[20] A.O. Macchiavelli *et al.*, Phys. Rev. C **58**, R621 (1998).